Check for updates

Journal of Sensor Science and Technology
Vol. 34, No. 1 (2025) pp. 1-7
http://dx.doi.org/10.46670/JSST.2025.34.1.1
pISSN 1225-5475/eISSN 2093-7563

Three-Dimensional Magnetic Particle Imaging Utilizing an Open-type System: A Feasibility Study

Jiyun Nan[1,*], Kim Tien Nguyen[2,*], Jong-Oh Park[2], Eunpyo Choi[1,+], and Jayoung Kim[3,+]

Abstract

Localization of magnetic nanoparticles is critical for precise intravascular therapy and drug delivery. Conventional magnetic particle imaging scanners are closed bore-type structures in which the working space is limited to the inside of the coil, leading to poor compatibility with other medical devices and limited user accessibility during operation. This paper presents an open-type magnetic particle imaging (OMPI) scanner that can monitor magnetic particles in three-dimensional space. The device integrates an asymmetric arrangement of soft-core electromagnetic coils and a single side for magnetic spectroscopy. The monitoring capabilities of the device were designed based on magnetic particle imaging technology. It is suitable for application with a concentration of magnetic particles of around 55.8 mg/mL within a region of interest of 30 × 30 × 30 mm^3. The imaging feasibility of this system was verified by in vitro experiments. The proposed system enables magnetic particle imaging to be applied more flexibly to complex medical scenarios.

Keywords: Targeted drug delivery, Magnetic particle imaging, Open-type MPI scanner

1. INTRODUCTION

Micro robotics has garnered significant interest as a multidisciplinary domain encompassing biology, mechanics, and materials science [1-3]. This interest is largely attributed to its potential applications in the medical and bioengineering sectors, such as targeted drug delivery, microsurgical procedures, and biosensing [4-6]. Within the medical realm, precise targeted delivery (PTD) holds great promise for cancer treatment by mitigating drug toxicity and resistance and enhancing the specificity of treatment protocols [7,8].

Microcarrier localization is pivotal in PTD. Among the various available biomedical imaging techniques, optical tracking, ultrasound imaging, X-ray monitoring, and magnetic resonance imaging (MRI) are frequently employed for in vivo microrobot tracking [9]. Magnetic particle imaging (MPI) is the most promising technique [10-13]. MPI is a tracer-based imaging modality that facilitates the tracking and quantification of materials such as magnetic nanoparticles (MNPs). The excitation and driving magnetic fields of the MPI scanner alter the magnetization of MNPs in the field-free region (FFR), and these changes are detected by the receiving coil. By analyzing the coil signal, we can deduce the position and concentration of the MNPs [14]. Since its inception in the early 2000s, MPI has undergone comprehensive advancements in scanner size, scanning trajectory, and system architecture [15-18]. The current MPI technology has a spatial resolution of 1 mm, temporal resolution of 65 frames per second, and sensitivity that is many times greater than that of MRI [19-21]. MPI scanners are broadly categorized into closed-bore, open-bore, and single-sided configurations, with closed-bore designs being the most commonly used structure [22-25]. Closed-bore MPI scanners can produce a homogeneous excitation field within the region of interest (ROI), but are limited by a confined workspace, reduced compatibility with other medical equipment, and limited user accessibility during operation. Open-type MPI scanners offer less penetration depth and less uniform excitation fields than closed designs, provide a more flexible workspace, and enable interaction with additional medical devices as their openness increases.

In this paper, we propose a method for tracking the position of

[1]School of Mechanical Engineering, Chonnam National University Gwangju 61186, Korea
[2]Korea Institute of Medical Microrobotics, Gwangju 61186, Korea
[3]Department of Biosystems Engineering, Chungbuk National University Cheongju 28644, Korea
*These authors contributed equally to this work.
[+]Corresponding author: eunpyochoi@jnu.ac.kr, jaya@cbnu.ac.kr
(Received: Dec. 9, 2024, Revised: Dec. 16, 2024, Accepted: Dec. 18, 2024)

This is an Open Access article distributed under the terms of the Creative Commons Attribution Non-Commercial License(https://creativecommons.org/licenses/by-nc/3.0/) which permits unrestricted non-commercial use, distribution, and reproduction in any medium, provided the original work is properly cited.

MNPs in 3-dimensional space using an open-type MPI scanner constructed with an anisotropic electromagnetic coil (AEMC) system, the open-type magnetic particle imaging (OMPI) technique. This is the first attempt to construct an OMPI scanner using an AEMC system. The AEMC system is composed of six coils with soft magnetic cores having an anisotropic arrangement in 3-dimensional space, whereas the RF coils use open-type magnetic particle spectroscopy (OMPS) [26]. The main contribution of this study is the development of an open-structure MPI scanner integrated with AEMC and OMPS, which will enable a more flexible application of MPI technology in medical treatment in the future. The performance of the proposed OMPI scanner is characterized using in vitro experiments to verify its feasibility of the proposed method.

2. OPEN-TYPE MAGNETIC PARTICLE IMAGING (OMPI)

MPI scanners are generally composed of two main components: electromagnetic coils capable of creating a Field-Free Point (FFP), and a Magnetic Particle Spectroscopy (MPS) system for detecting the magnetic particle signal. In this study, we employed an AEMC system consisting of six electromagnetic coils with soft magnetic cores to generate FFP, a specific type of FFR. The MPS system consists of excitation and reception units. Furthermore, an OMPI scanner was developed by integrating an OMPS with an AEMC system.

2.1 Generation of field-free point

To generate the FFP using the AEMC system, we employed an estimation method based on finite element modeling of the system [27-29]. The control equations for the magnetic field and its gradient at the target position P (x, y, z) are derived from the general control equations of a magnetic manipulation system. The equations used are as follows:

$$Q = \begin{bmatrix} B(P) \\ \hat{B}_x(P) \\ \hat{B}_y(P) \\ \hat{B}_z(P) \end{bmatrix} I = U(P)I \tag{1}$$

$$B(P) = \begin{bmatrix} B_{x,1}(P) & & B_{x,6}(P) \\ B_{y,1}(P) & \cdots & B_{y,6}(P) \\ B_{z,1}(P) & & B_{z,6}(P) \end{bmatrix} \tag{2}$$

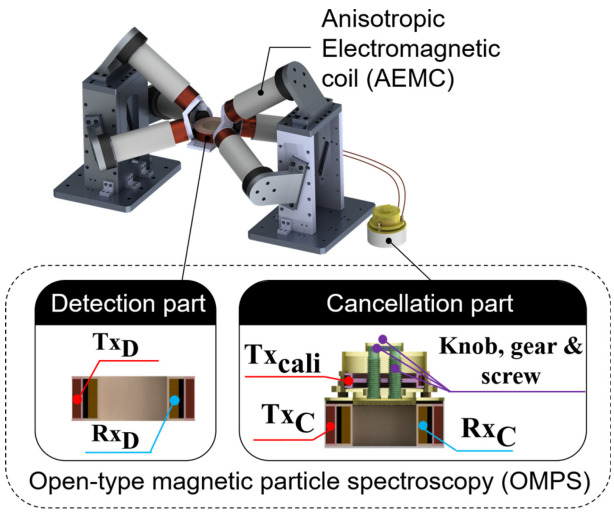

Fig. 1. The structure of OMPI scanner.

$$\hat{B}_j(P) = \begin{bmatrix} \frac{\partial \hat{B}_{j1}(P)}{\partial x} & & \frac{\partial \hat{B}_{j6}(P)}{\partial x} \\ \frac{\partial \hat{B}_{j1}(P)}{\partial y} & \cdots & \frac{\partial \hat{B}_{j6}(P)}{\partial y} \\ \frac{\partial \hat{B}_{j1}(P)}{\partial z} & & \frac{\partial \hat{B}_{j6}(P)}{\partial z} \end{bmatrix} \tag{3}$$

where, $I = [i_1 \ i_2 \ i_3 \ i_4 \ i_5 \ i_6]^T$, $U(P) \in R^{12\times6}$, $\hat{B}(P) \in R^{3\times6}$ is the unit current magnetic field of the 6 EMA coils, $\hat{B}_j(P)$ (j: x, y, z) $\in R^{3\times6}$ is the component of the field gradient of the magnetic field force along the x, y, and z directions. To obtain the current values required for the AEMC to generate the desired FFP at point *P*, we solved the linear equation of the pseudo-inverse of the unit current matrix **U** with the desired FFP condition matrix Q, following the equation mentioned in [30].

2.2 OMPI Scanning Strategy

The structure of the proposed OMPI scanner is shown in Fig. 1, where the two main components of the system are shown: AEMC and OMPS systems. The OMPS system includes both detection and cancellation. The detection part consists of a transmitter coil (T_{X_D}) and receiver coil (R_{X_D}), whereas the cancellation part consists of a compensation coil ($T_{X_{Cali}}$), cancellation coil (R_{X_C}), and duplicated transmitter coil (T_{X_C}). The MNPs located in the ROI generate fundamental harmonics at the same frequency (*f*) as the excitation field generated by R_{X_D} and higher harmonics at 2k+1 (k $\in N^+$) times the frequency of the fundamental harmonics as follows [31]:

$$u = \Sigma_i^n A_{2i+1} sin\{2\pi(2i+1)f \cdot t + \varphi\} \tag{4}$$

where, φ is the phase of the offset, A is the amplitude of the

harmonic, and A decreases as i increases. A typical MPI scanner uses higher harmonics to determine the signal of the MNPs because it is susceptible to interference from other materials at the fundamental harmonics. However, as the generation of detectable higher harmonics requires a high-amplitude excitation field, considerable power is consumed to operate the system. In addition, there is a risk that excitation fields of high amplitude produce adverse neural stimulation in organisms [22]. Therefore, we used a low-amplitude excitation field to excite the MNPs, although this reduced the sensitivity of the scanner and made it difficult to record the weak fundamental harmonic signals of the MNPs in dilute samples. Nevertheless, we applied the cancellation method to increase the sensitivity of the scanner as much as possible, and verified the sensitivity limitation through in vitro experiments. The AEMC system can generate an FFP at any specified location within the ROI; thus, the FFP can follow the user-input scan trajectory during scan imaging. In this study, the field of view (FOV) is 30 × 30 × 30 mm^3. To minimize the time required to complete single-location tracking, location tracking was performed twice. The range of the first tracking (global tracking) was the entire FOV with the FFP motion step in the x, y, and z directions of 3 mm, 5 mm, and 3 mm, respectively. At the end of global tracking, we obtained the position tracking results for the MNPs in three dimensions of 11 × 7 × 11 pixels. First, we determine the location where the maximum signal value is located and then specify that location as the center of the volume for the second tracking (so-called local tracking). In local tracking, the scanning range was 8 × 12 × 8 mm^3 and the FFP motion steps in the x, y, and z directions were 1 mm. At the end of local tracking, we obtained the results of position tracking for the MNPs in three dimensions with 9 × 13 × 9 pixels. Fig. 2 shows the scan range, data recording points, and the zigzag scanning path for global and local tracking.

In the OMPS system for detecting MNP signals, T_{X_D}, T_{X_C}, $T_{X_{Cali}}$ and a 21 nF capacitor are connected in series to construct a resonant circuit, where the current flow on T_{X_D} and $T_{X_{Cali}}$ in the opposite direction to T_{X_C}. Two Rx coils were connected in series, and the currents on the coils flowed in the same direction. The position of the calibration coil can be changed by turning the knob such that the inductive voltage signal on the Rx circuit can be canceled to zero as much as possible when the MNPs are not in position. The cross-sectional view in Fig. 1 shows the structure of the coils inside the detection and cancellation sections. In this work, the two Tx coils used as excitation units have a frequency of 11.8 kHz and an amplitude of 1 A, and the maximum peak amplitude of the magnetic field at the upper surface of the T_{X_D} coil is 2 mT. Some of the parameters of the scanner are shown in Table 1. In the Rx loop, we filtered the received signal using analog bandpass filters at 10.8 kHz and 12.8 kHz, and then amplified it 20 times using a preamplifier. The acquired digital signal is then filtered again on the PC using a digital bandpass filter at 10.8 kHz and 12.8 kHz. The connections between the devices comprising the entire system are illustrated in Fig. 3. We recorded the root-mean-square signal value at each pixel point in the FOV with the position information of the FFP at that location and finally reconstructed the scanned image from the recorded data. It takes approximately 550 ms to record each pixel once;

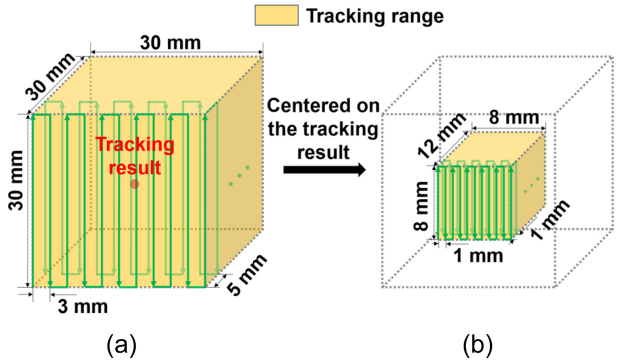

Fig. 2. (a) Scanning path and recording position of Global tracking. (b) Scanning path and recording position of local tracking.

Table 1. System Parameters

CATEGORY	PARAMETERS	VALUE
Magnetic gradient of FFP field	G	1 T/m
Amount of resovist particle	m_p	100 μL (55.8 mg/mL)
Max. Current of Tx coil	I_T	1 A_{pk}
Frequency of I_T	f	11.8 kHz

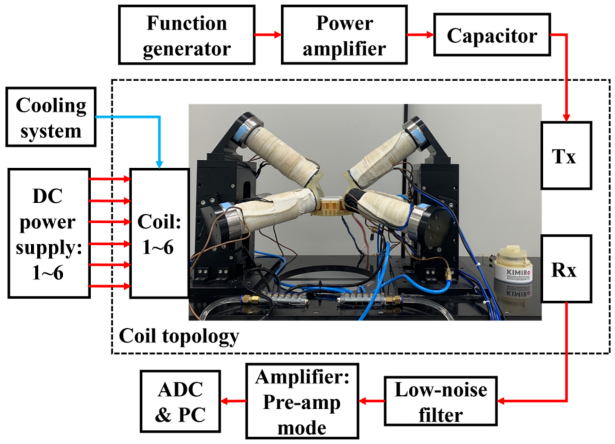

Fig. 3. Connect diagram of OMPI scanner and device.

therefore, it takes approximately 8 min to complete global tracking and 10 min to complete local tracking.

3. EXPERIMENTAL RESULTS

3.1 Experimental Setup

To validate the proposed position-tracking method, we performed in vitro experiments. In vitro experiments were conducted to evaluate the position-tracking accuracy of the OMPI scanner in 3D space. The MNPs used for OMPI were 100 µL of Resovist (Meito Sangyo Co. Ltd, Japan) with Fe concentration and magnetization rate of 55.8 mg/mL and 0.0308 c.g.s, respectively. The positioning jig was fabricated using a 3D printer (Object Eden 260VS, Stratasys, Korea) with an acrylic material (Veroclear, Stratasys, Korea). The DC power supplies for the EMA coil were three MX15s and three 3001iXs from AMETEK, USA. A VC 7000 (Lauda, Germany) cooling system was used to cool the EMA coils. The function generator and power amplifier that supplied power to the loop where the Tx coil was located were KEYSIGHT TECHNOLOGIES 33210A and AETECHRON 7224 from the United States of America, respectively. The low-noise filter used on the Rx was SR650 from Stanford Research Systems, United States of America, and the preamplifier was HSA 4014 from NF, Japan. The final analog-to-digital converter (ADC) used was a USB-6351 from NI, USA. On the PC, the software used to read, record, and analyze the data was LabView from NI and MATLAB from MathWorks, USA. A schematic of the device is shown in Fig. 4.

Fig. 4. (a) OMPI scanning system. (b) Function generator and power amplifier. (c) Low-noise filter, amplifier, and ADC. (d) The LabView interface on PC. (e) cooling system. (f) DC power supply.

3.2 Scanner Calibration

In contrast to conventional MPI scanners, the presence of cores in the AEMC of the OMPI scanner interferes with the MNPs signal, and the OMPS with an open structure improves the efficacy of the cores. Fig. 5 (a) shows the results when the MNPs were localized without any filtering operation. It can be seen that the signal of MNPs is completely masked by the interference signal. To eliminate interference from the cores, we added a scanning step for background interference before tracking the MNPs. First, when there are no MNPs, the FFP is scanned by the specified path, and the signal from the received coil is recorded as background interference data (as shown in Fig. 5 (b). Later, when MNPs were present, the same scanning was performed, and the background interference data were subtracted from the scanned data. Fig. 5 (c) shows the tracking results for the MNPs after eliminating background interference. Evidently, the removal of background interference has a significant influence on tracking results.

3.3 Three-dimensional Localization Performance

The container held 100 µL of undiluted resovist (~5.58 mg of Fe), and the positioning jig was employed to secure it. The height of the cylindrical container into which the MNPs were placed was

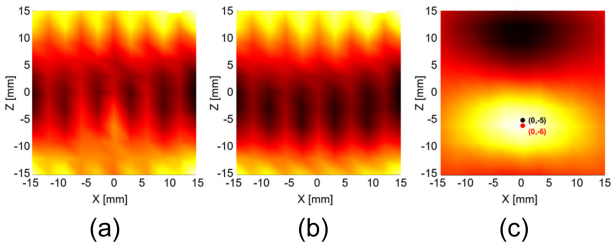

Fig. 5. Scanning image of MNPs placed at (0, 0, -5). (a) Before filtering, (b) Background noise, (c) After filtering.

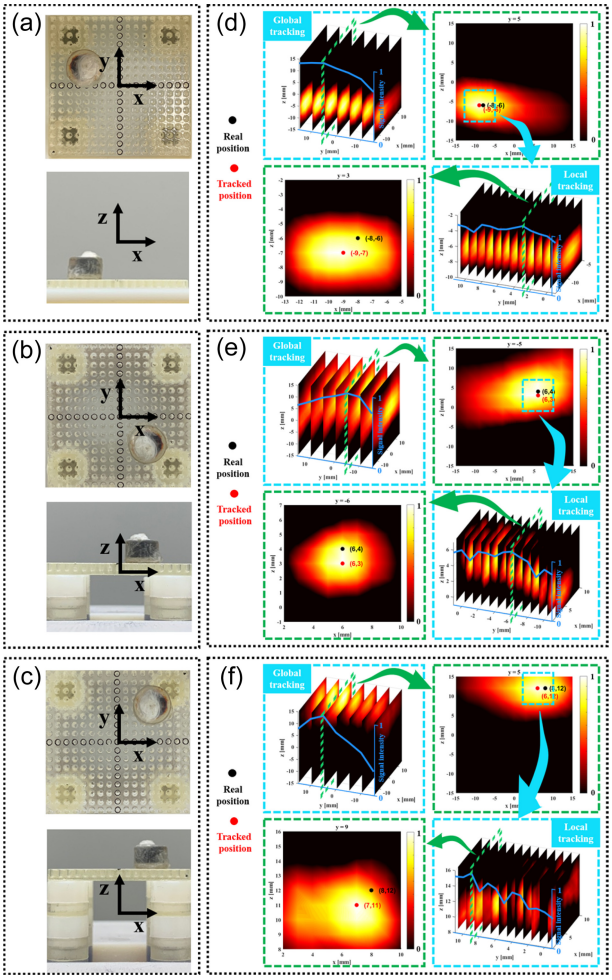

Fig. 6. Position tracking in 3D for 100 µL of Resovist. (a-c) The container filled with 100 µL Resovist are located at (-8, 4, -6), (6, -6, 4) and (8, 8, 12) respectively. (d-f) Results of global tracking and local tracking of MNPs at (-8, 4, -6), (6, -6, 4) and (8, 8, 12), respectively.

4 mm, and the diameter of the bottom circle was 6 mm. The positioning jig was divided into a support table (32 × 32 mm^2) that can fix the container at 2 mm intervals in the x- and y-directions and several gaskets that change the height of the support table, and the z-direction can be adjusted by changing the height of the support table.

We used this approach and placed MNPs at different locations for the tracking tests. Fig. 6 (a-c) show the real positions of the samples in three dimensions, named P1 (-8 mm, 4 mm, -6 mm), P2 (6 mm, -6 mm,4 mm), and P3 (8 mm, 8 mm, 12 mm). Fig. 6 (d-f) show the results of global tracking and local tracking for samples P1-P3. In this case, we performed a threshold process on the resulting data to remove the data below the median value from the original data. This process enhances the visualization of the results. If we take the position information corresponding to the maximum signal value of the local tracking result as the position tracking result, then the position tracking results of Fig. 6 (d-f) are t1: (-9 mm, 3 mm, -7 mm), t2: (6 mm, -6 mm,3 mm), t3: (7 mm, 9 mm, 11 mm), respectively. The root-mean-square errors along the x, y, and z axes for these three positions were 0.82 mm, 0.82 mm, 1 mm, and the standard deviations of the errors were 0.58 mm, 1 mm, and 0 mm, respectively.

4. DISCUSSIONS AND CONCLUSIONS

In this study, the proposed OMPI technique successfully demonstrated the feasibility of constructing open-type MPI systems using AEMC and OMPS. The accuracy of the OMPI scanner was validated through in vitro experiments. The anisotropic structure was used in combination with an iron core coil to improve the efficiency of generating the gradient magnetic field of the FFP, which resulted in a low power consumption of the entire OMPI system of 0.22 kW. Our scanner's sensitivity (278 µg Fe) is significantly lower than that of single-sided MPI (112 µg Fe) [24], as well as the closed-bore AM MPI (5 µg Fe) [21] and open-sided MPI (5.5 µg Fe) [23]. This disparity arises primarily from the pronounced effect of anisotropic coil noise, such as interference from the iron cores, in the open structural design. Enhancing the sensitivity is critical for OMPI scanners because of its direct impact on the penetration depth. The open design of the system rendered it particularly susceptible to interference from the AEMC cores. Although this study effectively visualized the MNP signals by mitigating background interference, the sensitivity remained inadequate for detecting highly diluted MNPs. Addressing this issue requires placing the elimination coil in the same environment as the excitation coil. Furthermore, signal improvement can be achieved by optimizing the coil design and employing a band-stop filter to retain the higher harmonics that are critical for imaging. In future studies, performance optimizations such as reducing the scanning time, increasing the sensitivity, and improving the accuracy are required to make the system more practical. We also aim to apply the OMPI scanner to various scenarios and focus on developing it for specific medical applications.

ACKNOWLEDGMENT

This work was supported by the Korea Medical Device Development Fund grant funded by the Korea government (the

Ministry of Science and ICT, the Ministry of Trade, Industry and Energy, the Ministry of Health & Welfare, the Ministry of Food and Drug Safety) (Project Number: 1415181807, RS-2021-KD000001), and by the Technology Innovation Program (or Industrial Strategic Technology Development Program) (20017903, Development of medical combination device for active precise delivery of embolic beads for transcatheter arterial chemoembolization and simulator for embolization training to cure liver tumor) funded By the Ministry of Trade, Industry & Energy (MOTIE, Korea).

REFERENCES

[1] Y. Chen, D. Chen, S. Liang, Y. Dai, X. Bai, B. Song, D. Zhang, H. Chen, and L. Feng, "Recent Advances in Field-Controlled Micro–Nano Manipulations and Micro–Nano Robots", *Adv. Intell. Syst.*, Vol. 4, No. 3, p. 2100116, 2022.

[2] L. Arcese, M. Fruchard, and A. Ferreira, "Adaptive Controller and Observer for a Magnetic Microrobot", *IEEE Trans. Robot.*, Vol. 29, No. 4, pp. 1060-1067, 2013.

[3] J. Jiang, Z. Yang, A. Ferreira, and L. Zhang, "Control and Autonomy of Microrobots: Recent Progress and Perspective", *Adv. Intell. Syst.*, Vol. 4, No. 5, p. 2100279, 2022.

[4] G. Go, S.-G. Jeong, A. Yoo, J. Han, B. Kang, S. Kim, K. T. Nguyen, Z. Jin, C.-S. Kim, Y. R. Seo, J. Y. Kang, J. Y. Na, E. K. Song, Y. Jeong, J. K. Seon, J.-O. Park, and E. Choi, "Human adipose–derived mesenchymal stem cell–based medical microrobot system for knee cartilage regeneration in vivo", *Sci. Robot.*, Vol. 5, No. 38, p. eaay6626, 2020.

[5] K. T. Nguyen, S.-J. Kim, H.-K. Min, M. C. Hoang, G. Go, B. Kang, J. Kim, E. Choi, A. Hong, J.-O. Park, and C.-S. Kim, "Guide-Wired Helical Microrobot for Percutaneous Revascularization in Chronic Total Occlusion in-Vivo Validation", *IEEE Trans. Biomed. Eng.*, Vol. 68, No. 8, pp. 2490-2498,2021.

[6] K. T. Nguyen, H. Kee, G. Go, S.-J. Kim, E. Choi, J.-O. Park, S. Park, and J. Kim, "Field-Free Region Scanning-Based Magnetic Microcarrier Targeting in Multibifurcation Vessels", *Adv. Intell. Syst.*, Vol. 6, No. 5, p. 2300700, 2024.

[7] M. T. Manzari, Y. Shamay, H. Kiguchi, N. Rosen, M. Scaltriti, and D. A. Heller, "Targeted drug delivery strategies for precision medicines", *Nat. Rev. Mater.*, Vol. 6, No. 4, pp. 351-370, 2021.

[8] W. Yu, R. Liu, Y. Zhou, and H. Gao, "Size-Tunable Strategies for a Tumor Targeted Drug Delivery System", *ACS Cent. Sci.*, Vol. 6, No. 2, pp. 100-116, 2020.

[9] B. Wang, Y. Zhang, and L. Zhang, "Recent progress on micro- and nano-robots: towards in vivo tracking and localization", *Quant. Imaging Med. Surg.*, Vol. 8, No. 5, pp. 461-479, 2018.

[10] B. Zheng, M. P. von See, E. Yu, B. Gunel, K. Lu, T. Vazin, D. V. Schaffer, P. W. Goodwill, and S. M. Conolly, "Quantitative Magnetic Particle Imaging Monitors the Transplantation, Biodistribution, and Clearance of Stem Cells In Vivo", *Theranostics*, Vol. 6, No. 3, pp. 291-301, 2016.

[11] E. Y. Yu, M. Bishop, B. Zheng, R. M. Ferguson, A. P. Khandhar, S. J. Kemp, K. M. Krishnan, P. W. Goodwill, and S. M. Conolly, "Magnetic Particle Imaging: A Novel in Vivo Imaging Platform for Cancer Detection", *Nano Lett.*, Vol. 17, No. 3, pp. 1648-1654, 2017.

[12] A. C. Bakenecker, M. Ahlborg, C. Debbeler, C. Kaethner, T. M. Buzug, and K. Lüdtke-Buzug, "Magnetic particle imaging in vascular medicine", *Innov. Surg. Sci.*, Vol. 3, No. 3, pp. 179-192, 2018.

[13] Z. W. Tay, P. Chandrasekharan, A. Chiu-Lam, D. W. Hensley, R. Dhavalikar, X. Y. Zhou, E. Y. Yu, P. W. Goodwill, B. Zheng, C. Rinaldi, and S. M. Conolly, "Magnetic Particle Imaging-Guided Heating in Vivo Using Gradient Fields for Arbitrary Localization of Magnetic Hyperthermia Therapy", *ACS Nano*, Vol. 12, No. 4, pp. 3699-3713, 2018.

[14] B. Gleich and J. Weizenecker, "Tomographic imaging using the nonlinear response of magnetic particles", *Nature*, Vol. 435, No. 7046, pp. 1214-1217, 2005.

[15] N. Panagiotopoulos, F. Vogt, J. Barkhausen, T. M. Buzug, R. L. Duschka, K. Lüdtke-Buzug, M. Ahlborg, G. Bringout, C. Debbeler, M. Gräser, C. Kaethner, J. Stelzner, H. Medimagh, and J. Haegele, "Magnetic particle imaging: current developments and future directions", *Int. J. Nanomedicine*, Vol. 10, p. 3097, 2015.

[16] T. Knopp, N. Gdaniec, and M. Möddel, "Magnetic particle imaging: from proof of principle to preclinical applications", *Phys. Med. Biol.*, Vol. 62, No. 14, pp. R124-R178, 2017.

[17] T. Knopp, S. Biederer, T. Sattel, J. Weizenecker, B. Gleich, J. Borgert, and T. M. Buzug, "Trajectory analysis for magnetic particle imaging", *Phys. Med. Biol.*, Vol. 54, No. 2, pp. 385-397, 2009.

[18] A. Neumann, K. Gräfe, A. von Gladiss, M. Ahlborg, A. Behrends, X. Chen, J. Schumacher, Y. Blancke Soares, T. Friedrich, H. Wei, A. Malhorta, E. Aderhold, A. C. Bakenecker, K. Lüdtke-Buzug, and T. M. Buzug, "Recent developments in magnetic particle imaging", *J. Magn. Magn. Mater.*, Vol. 550, p. 169037, 2022.

[19] O. C. Sehl and P. J. Foster, "The sensitivity of magnetic particle imaging and fluorine-19 magnetic resonance imaging for cell tracking", *Sci. Rep.*, Vol. 11, No. 1, p. 22198, 2021.

[20] L. C. Wu, Y. Zhang, G. Steinberg, H. Qu, S. Huang, M. Cheng, T. Bliss, F. Du, J. Rao, G. Song, L. Pisani, T. Doyle, S. Conolly, K. Krishnan, G. Grant, and M. Wintermark, "A Review of Magnetic Particle Imaging and Perspectives on Neuroimaging", *Am. J. Neuroradiol.*, Vol. 40, No. 2, pp. 206-212, 2019.

[21] N. Talebloo, M. Gudi, N. Robertson, and P. Wang, "Magnetic Particle Imaging: Current Applications in Biomedical Research", *J. Magn. Reson. Imaging*, Vol. 51, No. 6, pp. 1659-1668, 2020.

[22] T.-A. Le, M. P. Bui, and J. Yoon, "Development of Small-Rabbit-Scale Three-Dimensional Magnetic Particle Imaging System with Amplitude-Modulation-Based Reconstruction", *IEEE Trans. Ind. Electron.*, Vol. 70, No. 3, pp. 3167-3177, 2023.

[23] S.-M. Choi, J.-C. Jeong, J. Kim, E.-G. Lim, C. Kim, S.-J.

Park, D.-Y. Song, H.-J. Krause, H. Hong, and I. S. Kweon, "A novel three-dimensional magnetic particle imaging system based on the frequency mixing for the point-of-care diagnostics", *Sci. Rep.*, Vol. 10, No. 1, p. 11833, 2020.

[24] C. B. Top and A. Gungor, "Tomographic Field Free Line Magnetic Particle Imaging with an Open-Sided Scanner Configuration", *IEEE Trans. Med. Imaging*, Vol. 39, No. 12, pp. 4164-4173, 2020.

[25] Y. Blancke Soares, K. Lüdtke-Buzug, A. Von Gladiss, C. Debbeler, T. M. Buzug, and K. Gräfe, "Further system characterization of the Single-Sided MPI Scanner with two- and three-dimensional measurements", *Int. J. Magn. Part. Imaging*, Vol. 7, No. 2, 2021.

[26] C. Kim, J. Nan, J. Kim, J.-O. Park, and C.-S. Kim, "Open-Structure Magnetic Particle Spectroscopy (OMPS): Feasibility Study", *IEEE Magn. Lett.*, Vol. 13, pp. 1-5, 2022.

[27] K. Tien Nguyen, M. Phu Bui, T.-A. Le, V. Du Nguyen, J. Yoon, J.-O. Park, and J. Kim, "A magnetic particle imaging in anisotropic magnetic manipulation platform", *Measurement*, Vol. 208, p. 112391, 2023.

[28] C. Kim, J. Kim, J.-O. Park, E. Choi, and C.-S. Kim, "Localization and Actuation for MNPs Based on Magnetic Field-Free Point: Feasibility of Movable Electromagnetic Actuations", *Micromachines*, Vol. 11, No. 11, p. 1020, 2020.

[29] K. T. Nguyen, M. P. Bui, T.-A. Le, S. J. Kim, H. Y. Kim, J. Yoon, J.-O. Park, and J. Kim, "Magnetic particle image scanner based on asymmetric core-filled electromagnetic actuator", *Comput. Biol. Med.*, Vol. 169, p. 107864, 2024.

[30] M. C. Hoang, K. T. Nguyen, V. H. Le, J. Kim, E. Choi, B. Kang, J.-O. Park, and C.-S. Kim, "Independent Electromagnetic Field Control for Practical Approach to Actively Locomotive Wireless Capsule Endoscope", *IEEE Trans. Syst. Man Cybern. Syst.*, Vol. 51, No. 5, pp. 3040-3052, 2021.

[31] M. Graeser, T. Knopp, M. Grüttner, T. F. Sattel, and T. M. Buzug, "Analog receive signal processing for magnetic particle imaging: Analog receive signal processing for magnetic particle imaging", *Med. Phys.*, Vol. 40, No. 4, p. 042303, 2013.